Nuclear Science and Techniques (2025) 36:219
https://doi.org/10.1007/s41365-025-01794-1

Emergence of pygmy monopole strength in neutron-rich nickel isotopes

Shuai Sun[1] · Ya-Lu Wang[1] · Miao Qi[1] · Rong An[2] · Li-Gang Cao[1,3] · Feng-Shou Zhang[1,3,4]

Received: 24 January 2025 / Revised: 29 March 2025 / Accepted: 7 April 2025 / Published online: 12 September 2025

Abstract
The continuum quasiparticle random phase approximation (CQRPA), which includes the Skyrme interaction for both ground- and excited-state calculations, is extended in a more consistent manner in the present work. The emergence, evolution, and origin of pygmy monopole strengths along the even–even Ni isotopes were investigated carefully within consistent Skyrme HF + BCS and CQRPA models. The SLy5 Skyrme interaction and density-dependent zero-range pairing interactions were adopted in the calculations. No pygmy monopole strength was observed in $^{70-78}$Ni. However, pronounced pygmy monopole strengths are clearly observed in $^{80-84}$Ni, which are attributed mainly to the neutron excitations from weakly bound orbitals into the continuum. The neutron states involved in the pygmy monopole strength include $1g_{9/2}$, $2d_{5/2}$, $3s_{1/2}$ and $2d_{3/2}$. We suggest that more efforts from experimental investigations of pygmy monopole resonance should be made to confirm or disprove the predictions from models in the future.

Keywords Pygmy monopole resonance · Continuum quasiparticle random phase approximation · Skyrme energy density functional

1 Introduction

The multipole response and appearance of pygmy dipole resonance (PDR) in finite nuclei far from the β-stability line have become hot issues in nuclear physics [1, 2]. Pygmy dipole resonance, which corresponds to the collective motion between the neutron skin and saturated core, has gained considerable attention because of its important applications in nuclear astrophysics and nuclear physics [3–7]. For example, the PDR found in the isovector giant dipole resonance could have a pronounced effect on the neutron capture rate in *r*-process nucleosynthesis. The properties of PDR are also used to constrain the equation of state of asymmetric nuclear matter [8–12]; it plays similar role as the neutron skin in nuclear physics [13, 14].

PDR has been widely studied over the years, both experimentally and theoretically, using various methods [15–28]. In contrast, pygmy monopole resonance (PMR) has been much less analyzed experimentally in neutron-rich nuclei, and it has been theoretically predicted in neutron-rich Mg [29, 30], Ca [30–32], Ni [30, 33, 34], Sn, and Pb [35–37] isotopes. The calculations were based mainly on discretized quasiparticle random phase approximation (QRPA) or the finite amplitude method. It has been shown that PMR may significantly reduce the incompressibility in the nucleus with pronounced neutron excess, which could provide a more general and deeper understanding of nuclear incompressibility in isospin asymmetric systems [35]. Therefore,

This work was partly supported by the National Natural Science Foundation of China (Nos. 12275025, 11975096, 12135004, and 11961141004), and the Fundamental Research Funds for the Central Universities (No. 2020NTST06).

✉ Li-Gang Cao
caolg@bnu.edu.cn

1 Key Laboratory of Beam Technology of Ministry of Education, School of Physics and Astronomy, Beijing Normal University, Beijing 100875, China

2 School of Physics, Ningxia University, Yinchuan 750021, China

3 Key Laboratory of Beam Technology of Ministry of Education, Institute of Radiation Technology, Beijing Academy of Science and Technology, Beijing 100875, China

4 Center of Theoretical Nuclear Physics, National Laboratory of Heavy Ion Accelerator of Lanzhou, Lanzhou 730000, China

the measurement of isoscalar giant monopole resonances (ISGMR) and confirming the existence of PMR in neutron-rich nuclei are very important in nuclear physics. Following the suggestion of theoretical results, the ISGMR was measured by Vandebrouck et al. in the neutron-rich nucleus ^{68}Ni using inelastic α scattering at 50A MeV in inverse kinematics with the active target MAYA at GANIL [38, 39]. The pygmy monopole strength was observed at 12.9 MeV in addition to isoscalar giant monopole resonance. However, in the case of giant monopole resonance, excitations are usually built on the $2\hbar\omega$ particle–hole configurations, which indicates that the particle states involved in all low-energy monopole excitations may be embedded in the continuum. Thus, correct treatment of the continuum in a neutron-rich nucleus is required to explain the experimental results.

In Refs. [40, 41], the nonrelativistic and relativistic continuum random phase approximations (CRPA) with Green's function method were used to calculate the monopole strength distributions of ^{68,78}Ni, and the calculations indicated that there was no pronounced monopole state below the excitation energy of 20 MeV. Instead, a shoulder structure appeared in the low-energy region. This suggests that the discretized RPA may not be applicable to the calculation of the monopole response in ^{68}Ni, which should be replaced by the CRPA with Green's function method. CRPA calculations show that there is no PMR for ^{68,78}Ni. However, it is unclear whether PMR exists in more neutron-rich Ni isotopes. In this work, we focus on the evolution of ISGMR in neutron-rich Ni isotopes, particularly with respect to its low-energy strength.

The PMR in an open-shell nucleus cannot be accurately described by the CRPA with Green's function method because the pairing correlation is not considered. Hagino and Sagawa formulated a continuum quasiparticle random phase approximation (CQRPA) for open-shell nuclei in the coordinate space representation in Ref. [42]. The nucleon–nucleon interactions for the ground state adopted the Woods–Saxon type. For the residual interactions in the CQRPA calculations, they used the t_0 and t_3 parts of the Skyrme residual interactions. In this study, we extend the CQRPA model in Ref. [42] in a more consistent manner and applied it to study the ISGMR in neutron-rich Ni isotopes. In the new CQRPA model, the Schrödinger equation with a Woods–Saxon mean-field potential was replaced by the Hartree–Fock mean-field theory with the standard Skyrme interaction in the ground-state calculations. The Landau–Migdal forms of residual interactions derived from the Skyrme energy density functional (EDF) are adopted in the CQRPA calculations.

The remainder of this paper is organized as follows. In Sect. 2, we briefly introduce our theoretical framework. In Sect. 3, the CQRPA monopole strength distributions were investigated. The low-energy strengths of more neutron-rich Ni isotopes were studied carefully to explore the PMR. Finally, Sect. 4 provides summary and perspective.

2 Theoretical framework

In this work, the Skyrme Hartree–Fock + Bardeen–Cooper–Schrieffer (HF+BCS) and CQRPA methods were employed to study pygmy monopole resonance in neutron-rich nickel isotopes. The Skyrme interaction is expressed as an effective zero-range force between nucleons with density- and momentum-dependent terms, which has been successfully applied in the description of various nuclear properties [43, 44]. In this study, the Skyrme force SLy5 [45] was adopted for ground- and excited-state calculations. The pairing correlation is generated by a density-dependent zero-range force

$$V_{\text{pair}}(\mathbf{r}_1,\mathbf{r}_2) = V_0\left[1-\eta\left(\frac{\rho(\mathbf{r})}{\rho_0}\right)\right]\delta(\mathbf{r}_1-\mathbf{r}_2), \tag{1}$$

where $\rho(\mathbf{r})$ is the particle density and $\rho_0 = 0.16$ fm^{-3} is the density at nuclear saturation. η was set to 0.5, corresponding to a mixed pairing interaction. The pairing strength V_0 is fixed to be 483.5 MeV·fm^3 by reproducing the empirical neutron gap in ^{74}Ni (Δ_n=1.262 MeV) [46, 47]. This value was then extended to calculations of other nickel isotopes.

The CQRPA model is briefly reviewed as follows. Further details are provided in Ref. [42]. The CQRPA response function Π_{CQRPA} is governed by the Bethe–Salpeter (B–S) equation; its formalism generalized to the nuclear systems is given by

$$\Pi_{\text{CQRPA}} = \Pi_0 + \Pi_0 V_{\text{res}} \Pi_{\text{CQRPA}}, \tag{2}$$

where $\Pi_0(r,r';E)$ is the unperturbed response function, which can be given by

$$\begin{aligned}\Pi_0(r,r';E) = &-\sum_{\alpha\leq\beta} D_{\alpha\beta}(r)D_{\alpha\beta}(r')\left(\frac{1}{E_\alpha+E_\beta-E-i\eta}\right.\\ &\left.+\frac{1}{E_\alpha+E_\beta+E-i\eta}\right)\\ &-\sum_\alpha \phi_\alpha(r)\phi_\alpha(r')v_\alpha^2\sum_{j_k l_k}\langle j_\alpha l_\alpha\|Y_L\|j_k l_k\rangle^2\frac{1}{2L+1}\\ &\times\left\{\left\langle r\left|\frac{1}{E_\alpha+\hat{h}-\lambda-E-i\eta}\right.\right.\right.\\ &\left.+\frac{1}{E_\alpha+\hat{h}-\lambda+E-i\eta}\right|r'\Big\rangle\\ &-\sum_\beta \delta_{j_k j_\beta}\delta_{l_k,l_\beta}\phi_\beta(r)\phi_\beta(r')\\ &\left.\left(\frac{1}{E_\alpha+\varepsilon_\beta-\lambda-E-i\eta}+\frac{1}{E_\alpha+\varepsilon_\beta-\lambda+E-i\eta}\right)\right\},\end{aligned} \tag{3}$$

where v_α^2, E_α, and ϕ_α are the occupation probability, quasiparticle energy, and radial wavefunction of the quasiparticle state α, respectively. $D_{\alpha\beta}(r)$ is the matrix element expressed as

$$D_{\alpha\beta}(r) = \phi_\alpha(r)\phi_\beta(r)\langle j_\alpha l_\alpha||Y_L||j_\beta l_\beta\rangle \frac{u_\alpha v_\beta + (-)^L v_\alpha u_\beta}{\sqrt{2L+1}}(1+\delta_{\alpha,\beta})^{-1/2}. \tag{4}$$

In Eq. (3), the first term represents the two-quasiparticle excitations within the pairing active space, whereas the second term corresponds to the transitions from the inside to the outside of the pairing active space. The terms V_{res} in Eq. (2) are the residual interactions in the B–S equation, which are from the second derivative of the Skyrme EDF with respect to the proton and neutron densities and are expressed by the Landau–Migdal parameters [48] in this study.

The monopole strength distribution $S(E)$ of the system to an external field $V_{\text{ext}}(\boldsymbol{r}) = r^2 Y_{\text{LM}}(\hat{\boldsymbol{r}})$ is then given by

$$S(E) = \frac{1}{\pi}\,\text{Im}\int \mathrm{d}r\mathrm{d}r' V_{\text{ext}}(r)\Pi\left(r,r';E\right)V_{\text{ext}}\left(r'\right). \tag{5}$$

After that, various moments can be calculated by means of the equation

$$m_k = \int E^k S(E)\mathrm{d}E; \tag{6}$$

then, one can obtain the constrained energy E_{con} and centroid energy E_{cen}

$$E_{\text{con}} = \sqrt{\frac{m_1}{m_{-1}}}, \quad E_{\text{cen}} = \frac{m_1}{m_0}. \tag{7}$$

Besides, the ratio of m_k for the low-energy (LE) PMR to the total strength, namely

$$R \equiv \frac{\int_0^{E_{\text{LE}}} E^k S(E)\mathrm{d}E}{\int_0^{E_{\max}} E^k S(E)\mathrm{d}E}, \tag{8}$$

is defined to quantify the evolution of the PMR with neutron excess, where E_{LE} is set to 11 MeV and $E_{\max}$ is equal to 40 MeV.

3 Results and discussion

First, we briefly discuss the ground-state properties of the nickel isotopes. The ground-state properties of finite nuclei are depicted using the HF+BCS method [50–52]. The HF+BCS equation is solved in coordinate space, where the radial size is set to 20 fm, which guarantees that the results under study are stable.

Table 1 shows the binding energies per nucleon, the neutron (proton) separation energies, charge radii, and neutron Fermi energies in even–even $^{68-84}$Ni isotopes calculated by using the SLy5 Skyrme interaction; meanwhile, the calculated results are compared with the corresponding experimental data.

It can be seen that the binding energies per nucleon decrease with increasing mass number, and the calculated values can reproduce the measurements well. The neutron separation energies of $^{68-82}$Ni predicted by the Skyrme EDF are somewhat smaller than the experimental data, but the calculated results can reproduce the data tendency with respect to the mass number well. In Table 1, it is shown that the theoretical proton separation energies S_{p} are in good agreement with the experimental data. We also show the calculated charge radii of even–even $^{68-84}$Ni isotopes in the table, which increase with increasing mass number. For the studied nuclei, only two nuclei, ^{68,70}Ni, had experimental charge radii data. These results were well reproduced by the calculations. The calculated neutron Fermi energies are presented in the last column of Table 1; one can see that the neutron Fermi energies are approaching to zero when the nuclei are becoming more and more unstable.

For neutron-rich nickel nuclei, the discretized RPA has been proved to be unreliable, whereas Green's function technique can properly take into account the contribution from the continuum [40, 41]. Therefore, CQRPA was adopted to explore the PMR in more neutron-rich Ni isotopes in the present study. As mentioned above, the residual interactions in the CQRPA calculations adopt the Migdal form. This means that the interactions used in CQRPA are not the same as those used in the ground-state calculations. We adjusted the residual interactions to ensure that a spurious isoscalar dipole state appeared at zero excitation energy, and the value of the renormalization factor was approximately 0.8.

Table 1 Binding energies per nucleon E_{b} (MeV), the neutron (proton) separation energies S_{n} (S_{p}) (MeV), charge radii R_{ch} (fm), and neutron Fermi energies λ_{n} (MeV) in even–even nickel isotopes from ^{68}Ni to ^{84}Ni, calculated by using SLy5 interaction. Corresponding experimental data are shown in the brackets for comparison [47, 49]

	E_{b} (MeV)	S_{n} (MeV)	S_{p} (MeV)	R_{ch} (fm)	λ_{n} (MeV)
^{68}Ni	8.71(8.68)	6.99(7.79)	14.47(15.43)	3.91(3.89)	−7.09
^{70}Ni	8.64(8.60)	6.11(7.31)	15.76(16.12)	3.93(3.91)	−6.24
^{72}Ni	8.56(8.52)	5.45(6.89)	17.04(17.15)	3.95	−5.62
^{74}Ni	8.46(8.43)	4.95(6.66)	18.29(18.02)	3.96	−5.13
^{76}Ni	8.36(8.34)	4.53(6.02)	19.50(18.92)	3.98	−4.70
^{78}Ni	8.26(8.24)	3.29(5.60)	20.69(20.26)	3.99	−2.40
^{80}Ni	8.10(8.09)	1.70(3.15)	21.46	4.01	−1.86
^{82}Ni	7.94(7.94)	1.44(2.70)	22.18	4.03	−1.60
^{84}Ni	7.78	1.11	22.85	4.04	−1.17

The CQRPA monopole strength distributions for $^{70-84}$Ni are shown in Fig. 1. One can see the monopole strengths for $^{70-78}$Ni increased monotonically from the particle threshold to the ISGMR peak at approximately 21 MeV. This implies that a shoulder structure appears in the low-energy region for $^{70-78}$Ni. This is consistent with the conclusions of Refs. [40, 41]; there is no PMR for $^{70-78}$Ni. However, starting from ^{80}Ni, the particle threshold becomes much lower, and an obvious PMR emerges in the energy region between 2.5 and 11 MeV. With the increasing of mass number, the low-energy strength becomes more and more strong.

We separated the low-energy PMR from the giant monopole resonance at an excitation energy of $E = 11$ MeV and calculated the ratios of the low-energy strength to the whole ISGMR strength for the non-energy-weighted sum rule m_0, inverse energy-weighted sum rule m_{-1}, and energy-weighted sum rule m_1, respectively. As illustrated in Fig. 2a, the ratios of m_0 (orange circles), m_{-1} (purple squares), and m_1 (black stars) of the low-energy strength are almost zero until mass number $A = 78$. From ^{80}Ni, the three ratios increased significantly, and the values became larger in more neutron-rich nuclei. This suggests that the contribution of the PMR below 11 MeV increases with increasing mass number. The centroid energies $E_{\rm cen}$ (green pentagons) and constrained energies $E_{\rm con}$ (pink triangles) are plotted as functions of the mass number in Fig. 2b, which is similar to Fig. 2a, the values of $E_{\rm cen}$ and $E_{\rm con}$ remain constant when the mass number is not greater than 78, whereas the two energies are significantly decreased from ^{80}Ni to ^{84}Ni because of the appearance and enhancement of the low-energy monopole strengths. The values of $E_{\rm cen}$ are somewhat higher than those of $E_{\rm con}$ along the Ni isotopic chain, especially for $^{80-84}$Ni.

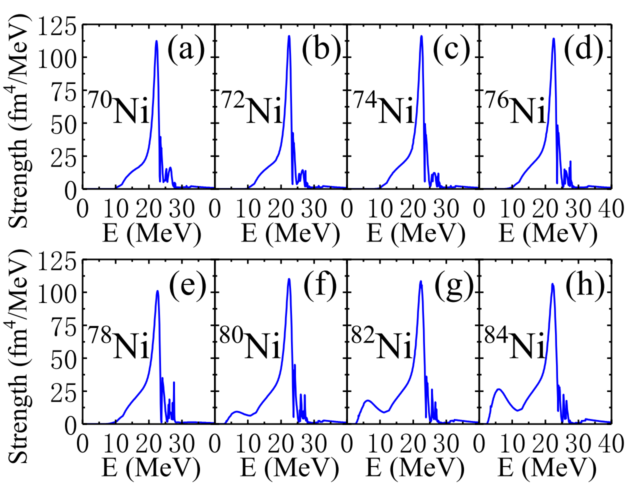

Fig. 1 (Color online) CQRPA monopole strength distributions for $^{70-84}$Ni predicted by the SLy5 Skyrme interaction

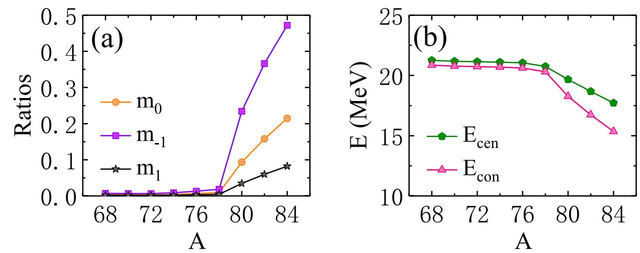

Fig. 2 (Color online) **a** Ratios R of m_0, m_{-1}, and m_1 for the even–even nickel isotopes from ^{68}Ni to ^{84}Ni. **b** Centroid energies $E_{\rm cen}$ and constrained energies $E_{\rm con}$ in $^{68-84}$Ni

In this paragraph, quasiparticle excitations in the low-energy region will be carefully investigated because these excitations may contribute significantly to the PMR strengths. The unperturbed and CQRPA monopole strengths of $^{80-84}$Ni are shown in Fig. 3a–c. For the giant monopole resonance, the CQRPA strengths are shifted down to a lower energy compared to the distribution of unperturbed strengths because the attractive residual interactions play an important role in isoscalar monopole excitation. The PMR strengths were slightly reduced compared to the unperturbed strengths, but the locations were almost unchanged. It can be seen that the low-energy strengths are highly sensitive to neutron excess. It was found that the low-energy strength below 20 MeV shown in the figures is made of the excitations mainly contributed by neutron states around the Fermi level, including $1g_{9/2}$, $2d_{5/2}$, $3s_{1/2}$, and $2d_{3/2}$. The corresponding single-particle energies $E_{\rm s.p.}$, gaps Δ, quasiparticle

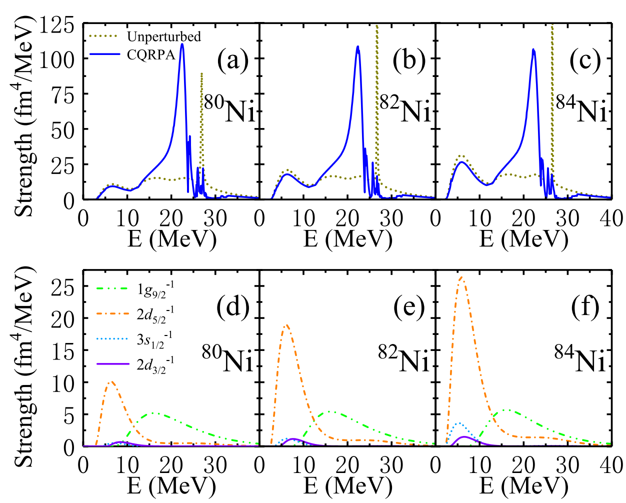

Fig. 3 (Color online) **a-c**: The unperturbed and CQRPA monopole strength distributions for $^{80-84}$Ni predicted by the SLy5 Skyrme interaction. **d-f**: Some unperturbed neutron threshold strengths, which contribute appreciably to the total unperturbed strength below 20 MeV in $^{80-84}$Ni, are shown for respective occupied orbits, $(1g_{9/2})^{-1}$, $(2d_{5/2})^{-1}$, $(3s_{1/2})^{-1}$, and $(2d_{3/2})^{-1}$

Table 2 Single-particle energies ($E_{s.p.}$ in MeV), gaps (Δ in MeV), quasiparticle energies ($E_{q.p.}$ in MeV), and occupation probabilities (v^2) of neutron states around the Fermi level in $^{80-84}$Ni, calculated by using SLy5 Skyrme interaction

	^{80}Ni				^{82}Ni				^{84}Ni			
State	$E_{s.p.}$	Δ	$E_{q.p.}$	v^2	$E_{s.p.}$	Δ	$E_{q.p.}$	v^2	$E_{s.p.}$	Δ	$E_{q.p.}$	v^2
$1g_{9/2}$	−5.80	0.73	4.01	0.99	−5.94	0.77	4.41	0.99	−6.08	0.57	4.94	1.00
$2d_{5/2}$	−1.62	0.67	0.72	0.33	−1.81	0.72	0.75	0.64	−2.01	0.53	0.99	0.92
$3s_{1/2}$	−0.40	0.4	1.52	0.02	−0.59	0.45	1.11	0.04	−0.78	0.38	0.55	0.14
$2d_{3/2}$	0.34	0.55	2.28	0.01	0.13	0.61	1.84	0.03	−0.08	0.45	1.18	0.04

energies $E_{q.p.}$, and occupation probabilities v^2 are listed in Table 2. We noticed that the single-particle energies of the four neutron states become increasingly bound with an increase in the neutron excess. It is shown that the gaps of the four neutron states are rather stable at approximately 0.6 MeV. The neutron states $2d_{5/2}$ are just above or below the Fermi energies; therefore, the quasiparticle energies are relatively small. As for states $1g_{9/2}$, $3s_{1/2}$ and $2d_{3/2}$, they are a little far from the Fermi energies, and their quasiparticle energies are relatively large except for state $3s_{1/2}$ in ^{84}Ni, because its single-particle energy is much closer to the Fermi energy. One can see that the occupation probabilities of $1g_{9/2}$ are almost 1.0, leading to relatively stable excitations. Other partially occupied orbits ($2d_{5/2}$, $3s_{1/2}$ and $2d_{3/2}$) changed their occupation probabilities when the neutron excess was increased. The corresponding unperturbed neutron threshold strengths, contributed by the excitation of neutrons around the Fermi surface to the continuum, are gradually enhanced[see Fig. 3d–f]: The occupancy probabilities of $2d_{5/2}$ are increased much more than the other states with the filling of neutrons, from 0.33 in ^{80}Ni increased to 0.92 in ^{84}Ni. Therefore, the increase in low-energy strengths in $^{80-84}$Ni is mainly due to the contribution of a stronger threshold strength of $2d_{5/2}$.

4 Summary and perspectives

In the present study, we extended the CQRPA approach in Ref. [42] in a more consistent manner, in which the model includes the Skyrme interaction for both ground- and excited-state calculations. Then, the consistent Skyrme HF+BCS and CQRPA models were applied to explore the emergence, evolution, and origin of low-energy monopole strengths along the even–even Ni isotopes. Shoulder structures at low-energy region for $^{70-78}$Ni are found, which are similar to the conclusions in Refs.[40, 41]. However, the situation changed dramatically with the occupation of the weakly bound neutron orbitals. Indeed, starting from ^{80}Ni, pronounced pygmy monopole strengths were clearly identified. The origin of the low-energy monopole strength is attributed to neutron excitations from the weakly bound orbitals into the continuum, including neutron states $1g_{9/2}$, $2d_{5/2}$, $3s_{1/2}$, and $2d_{3/2}$. The changes in the ratios of low-energy strengths to total ISGMR strengths for m_{-1}, m_0 and m_1 as well as the centroid and constrained energies along Ni isotopes are also discussed, and the changes are more obvious when the mass numbers are larger than 78, which are attributed mainly to the emergence of low-energy strengths. Eventually, the experimental data of PMR in neutron-rich nuclei are obviously inadequate; more efforts from the experimental investigations of PMR shall be made to confirm or disprove the predictions from models in the future.

Author Contributions All authors contributed to the study conception and design. Material preparation, data collection, and analysis were performed by Shuai Sun and Li-Gang Cao. The first draft of the manuscript was written by Shuai Sun, and all authors commented on previous versions of the manuscript. All authors read and approved the final manuscript.

Declarations

Conflicts of Interest Feng-Shou Zhang is an editorial board member for Nuclear Science and Techniques and was not involved in the editorial review, or the decision to publish this article. All authors declare that there are no Conflict of interest.

References

1. N. Paar, D. Vretenar, E. Khan et al., Exotic modes of excitation in atomic nuclei far from stability. Rep. Prog. Phys. **70**, R02 (2007). https://doi.org/10.1088/0034-4885/70/5/R02
2. D. Savran, T. Aumann, A. Zilges, Experimental studies of the Pygmy Dipole Resonance. Prog. Part. Nucl. Phys. **70**, 210 (2013). https://doi.org/10.1016/j.ppnp.2013.02.003
3. E. Litvinova, H.P. Loens, K. Langanke et al., Low-lying dipole response in the relativistic quasiparticle time blocking approximation and its influence on neutron capture cross sections. Nucl. Phys. A **823**, 26 (2009). https://doi.org/10.1016/j.nuclphysa.2009.03.009
4. N. Tsoneva, S. Goriely, H. Lenske et al., Pygmy resonances and radiative nucleon captures for stellar nucleosynthesis. Phys. Rev. C **91**, 044318 (2015). https://doi.org/10.1103/PhysRevC.91.044318
5. T. Saito, M. Matsuo, Continuum random-phase approximation for (n,γ) reactions on neutron-rich nuclei: collective effects and resonances. Phys. Rev. C **107**, 064607 (2023). https://doi.org/10.1103/PhysRevC.107.064607
6. B.S. Cai, C.X. Yuan, Random forest-based prediction of decay modes and half-lives of superheavy nuclei. Nucl. Sci. Tech. **34**, 204 (2023). https://doi.org/10.1007/s41365-023-01354-5

7. P. Jiao, Z.R. Hao, Q.K. Sun et al., Measurements of ^{27}Al(γ, n) reaction using quasi-monoenergetic γ beams from 13.2 to 21.7 MeV at SLEGS. Nucl. Sci. Tech. **36**, 66 (2025). https://doi.org/10.1007/s41365-025-01662-y
8. A. Klimkiewicz, N. Paar, P. Adrich et al., Nuclear symmetry energy and neutron skins derived from pygmy dipole resonances. Phys. Rev. C **76**, 051603(R) (2007). https://doi.org/10.1103/PhysRevC.76.051603
9. A. Carbone, G. Colò, A. Bracco et al., Constraints on the symmetry energy and neutron skins from pygmy resonances in ^{68}Ni and ^{132}Sn. Phys. Rev. C **81**, 041301(R) (2010). https://doi.org/10.1103/PhysRevC.81.041301
10. V. Baran, M. Colonna, M. Di Toro et al., Connecting the pygmy dipole resonance to the neutron skin. Phys. Rev. C **88**, 044610 (2013). https://doi.org/10.1103/PhysRevC.88.044610
11. L. Liu, Y.W. Lu, S. Sun et al., Constraining symmetry energy from pygmy dipole resonances in ^{68}Ni and ^{132}Sn. Chin. Phys. C **49**, 024101 (2025). https://doi.org/10.1088/1674-1137/ad9016
12. L.G. Cao, Z.Y. Ma, Symmetry energy and isovector giant dipole resonance in finite nuclei. Chin. Phys. Lett. **25**, 1625 (2008). https://doi.org/10.1088/0256-307X/25/5/028
13. M.Q. Ding, D.Q. Fang, Y.G. Ma, Neutron skin and its effects in heavy-ion collisions. Nucl. Sci. Tech. **35**, 211 (2024). https://doi.org/10.1007/s41365-024-01584-1
14. R. An, S. Sun, L.G. Cao et al., New quantification of symmetry energy from neutron skin thicknesses of ^{48}Ca and ^{208}Pb. Nucl. Sci. Tech. **35**, 182 (2024). https://doi.org/10.1007/s41365-024-01551-w
15. P. Adrich, A. Klimkiewicz, M. Fallot et al., Evidence for Pygmy and Giant Dipole Resonances in ^{130}Sn and ^{132}Sn. Phys. Rev. Lett. **95**, 132501 (2005). https://doi.org/10.1103/PhysRevLett.95.132501
16. J. Gibelin, D. Beaume, T. Motobayashi et al., Decay pattern of pygmy states observed in neutron-rich ^{26}Ne. Phys. Rev. Lett. **101**, 212503 (2008). https://doi.org/10.1103/PhysRevLett.101.212503
17. O. Wieland, A. Bracco, F. Camera et al., Search for the Pygmy Dipole Resonance in ^{68}Ni at 600 MeV/nucleon. Phys. Rev. Lett. **102**, 092502 (2009). https://doi.org/10.1103/PhysRevLett.102.092502
18. T. Inakura, T. Nakatsukasa, K. Yabana, Emergence of pygmy dipole resonances: magic numbers and neutron skins. Phys. Rev. C **84**, 021302(R) (2011). https://doi.org/10.1103/PhysRevC.84.021302
19. K. Wang, M. Kortelainen, J.C. Pei, Probing surface quantum flows in deformed pygmy dipole modes. Phys. Rev. C **96**, 031301(R) (2017). https://doi.org/10.1103/PhysRevC.96.031301
20. D. Gambacurta, M. Grasso, O. Vasseur, Electric dipole strength and dipole polarizability in ^{48}Ca within a fully self-consistent second random-phase approximation. Phys. Lett. B **777**, 163 (2018). https://doi.org/10.1016/j.physletb.2017.12.026
21. E.G. Lanza, L. Pellegri, A. Vitturi et al., Theoretical studies of pygmy resonances. Prog. Part. Nucl. Phys. **129**, 104006 (2023). https://doi.org/10.1016/j.ppnp.2022.104006
22. D. Yang, L.G. Cao, Y. Tian et al., Importance of self-consistency in relativistic continuum random-phase approximation calculations. Phys. Rev. C **82**, 054305 (2010). https://doi.org/10.1103/PhysRevC.82.054305
23. L.G. Cao, Z.Y. Ma, Soft dipole modes in neutron-rich Ni-isotopes in QRRPA. Mod. Phys. Lett. A **19**, 2845 (2004). https://doi.org/10.1142/S0217732304015233
24. S. Sun, R.Q. Yu, L.G. Cao et al., Application of relativistic continuum random phase approximation to giant dipole resonance of ^{208}Pb and ^{132}Sn. Eur. Phys. J. A **60**, 61 (2024). https://doi.org/10.1140/epja/s10050-024-01288-5
25. D. Vretenar, N. Paar, P. Ring et al., Pygmy dipole resonances in the relativistic random phase approximation. Phys. Rev. C **63**, 047301 (2001). https://doi.org/10.1103/PhysRevC.63.047301
26. H. Lv, S.S. Zhang, Z.H. Zhang et al., Pygmy and giant dipole resonances in proton-rich nuclei ^{17,18}Ne. Chin. Phys. Lett. **34**, 082101 (2017). https://doi.org/10.1088/0256-307X/34/8/082101
27. K. Yoshida, N.V. Giai, Low-lying dipole resonance in neutron-rich Ne isotopes. Phys. Rev. C **78**, 014305 (2008). https://doi.org/10.1103/PhysRevC.78.014305
28. M. Martini, S. Péru, M. Dupuis, Low-energy dipole excitations in neon isotopes and N=16 isotones within the quasiparticle random-phase approximation and the Gogny force. Phys. Rev. C **83**, 034309 (2011). https://doi.org/10.1103/PhysRevC.83.034309
29. J.C. Pei, M. Kortelainen, Y.N. Zhang et al., Emergent soft monopole modes in weakly bound deformed nuclei. Phys. Rev. C **90**, 051304 (2014). https://doi.org/10.1103/PhysRevC.90.051304
30. F. Mercier, J.-P. Ebran, E. Khan, Low-energy monopole strength in spherical and axially deformed nuclei: cluster and soft modes. Phys. Rev. C **105**, 034343 (2022). https://doi.org/10.1103/PhysRevC.105.034343
31. J. Piekarewicz, Emergence of low-energy monopole strength in the neutron-rich calcium isotopes. Phys. Rev. C **96**, 044314 (2017). https://doi.org/10.1103/PhysRevC.96.044314
32. D. Gambacurta, M. Grasso, O. Sorlin, Soft breathing modes in neutron-rich nuclei with the subtracted second random-phase approximation. Phys. Rev. C **100**, 014317 (2019). https://doi.org/10.1103/PhysRevC.100.014317
33. E. Khan, N. Paar, D. Vretenar, Low-energy monopole strength in exotic nickel isotopes. Phys. Rev. C **84**, 051301 (2011). https://doi.org/10.1103/PhysRevC.84.051301
34. X. Sun, Evolution of soft monopole mode in the even-even nickel isotopes $^{58-68}$Ni. Phys. Rev. C **103**, 044603 (2021). https://doi.org/10.1103/PhysRevC.103.044603
35. E. Khan, N. Paar, D. Vretenar et al., Incompressibility of finite fermionic systems: stable and exotic atomic nuclei. Phys. Rev. C **87**, 064311 (2013). https://doi.org/10.1103/PhysRevC.87.064311
36. H.Z. Liang, T. Nakatsukasa, Z.M. Niu et al., Feasibility of the finite-amplitude method in covariant density functional theory. Phys. Rev. C **87**, 054310 (2013). https://doi.org/10.1103/PhysRevC.87.054310
37. Z.Z. Li, Y.F. Niu, G. Colò, Toward a unified description of isoscalar giant monopole resonances in a self-consistent quasiparticle-vibration coupling approach. Phys. Rev. Lett. **131**, 082501 (2023). https://doi.org/10.1103/PhysRevLett.131.082501
38. M. Vandebrouck, J. Gibelin, E. Khan et al., Measurement of the isoscalar monopole response in the neutron-rich nucleus ^{68}Ni. Phys. Rev. Lett. **113**, 032504 (2014). https://doi.org/10.1103/PhysRevLett.113.032504
39. M. Vandebrouck, J. Gibelin, E. Khan et al., Isoscalar response of ^{68}Ni to α-particle and deuteron probes. Phys. Rev. C **92**, 024316 (2015). https://doi.org/10.1103/PhysRevC.92.024316
40. I. Hamamoto, H. Sagawa, Self-consistent Hartree-Fock and RPA Green's function method indicate no pygmy resonance in the monopole response of neutron-rich Ni isotopes. Phys. Rev. C **90**, 031302 (2014). https://doi.org/10.1103/PhysRevC.90.031302
41. J. Piekarewicz, Nuclear breathing mode in neutron-rich nickel isotopes: sensitivity to the symmetry energy and the role of the continuum. Phys. Rev. C **91**, 014303 (2015). https://doi.org/10.1103/PhysRevC.91.014303
42. K. Hagino, H. Sagawa, Continuum QRPA in the coordinate space representation. Nucl. Phys. A **695**, 82 (2001). https://doi.org/10.1016/S0375-9474(01)01122-8
43. M. Bender, P.H. Heenen, P.G. Reinhard, Self-consistent mean-field models for nuclear structure. Rev. Mod. Phys. **75**, 121 (2003). https://doi.org/10.1103/RevModPhys.75.121

44. G. Colò, L.G. Cao, N.V. Giai et al., Self-consistent RPA calculations with Skyrme-type interactions: The skyrme_rpa program. Comput. Phys. Commun. **184**, 142 (2013). https://doi.org/10.1016/j.cpc.2012.07.016
45. E. Chabanat, P. Bonche, P. Haensel et al., A Skyrme parametrization from subnuclear to neutron star densities Part II. Nuclei far from stabilities. Nucl. Phys. A **635**, 231 (1998). https://doi.org/10.1016/S0375-9474(98)00180-8
46. S.A. Changizi, C. Qi, R. Wyss, Empirical pairing gaps, shell effects, and di-neutron spatial correlation in neutron-rich nuclei. Nucl. Phys. A **940**, 210 (2015). https://doi.org/10.1016/j.nuclphysa.2015.04.010
47. M. Wang, W.J. Huang, F.G. Kondev et al., The AME 2020 atomic mass evaluation (II). Tables, graphs and references. Chin. Phys. C **45**, 030003 (2021). https://doi.org/10.1088/1674-1137/abddaf
48. K.F. Liu, H.D. Luo, Z.Y. Ma et al., Skyrme-Landau parameterization of effective interactions: (II). Self-consistent description of giant multipole resonances. Nucl. Phys. A **534**, 25 (1991). https://doi.org/10.1016/0375-9474(91)90556-L
49. S. Malbrunot-Ettenauer, S. Kaufmann, S. Bacca et al., Nuclear charge radii of the nickel isotopes $^{58-68,70}$Ni. Phys. Rev. Lett. **128**, 022502 (2022). https://doi.org/10.1103/PhysRevLett.128.022502
50. P. Ring, P. Schuck, *The Nuclear Many-Body Problem* (Springer-Verlag, New York, 1980)
51. L.G. Cao, H. Sagawa, G. Colò, Microscopic study of the isoscalar giant monopole resonance in Cd, Sn, and Pb isotopes. Phys. Rev. C **86**, 054313 (2012). https://doi.org/10.1103/PhysRevC.86.054313
52. S. Sun, S.S. Zhang, Z.H. Zhang et al., Effect of pairing correlation on low-lying quadrupole states in Sn isotopes. Chin. Phys. C **45**, 094101 (2021). https://doi.org/10.1088/1674-1137/ac0b39